The Effect of Clouds as an Additional Opacity Source on the Inferred Metallicity of Giant Exoplanets

Anna Julia Poser [1,*], **Nadine Nettelmann [2]** and **Ronald Redmer [1]**

1   Institut für Physik, Universität Rostock, D-18051 Rostock, Germany; ronald.redmer@uni-rostock.de
2   Institut für Planetenforschung, Deutsches Zentrum für Luft- und Raumfahrt (DLR) Berlin,
    D-12489 Berlin, Germany; nadine.nettelmann@dlr.de
*   Correspondence: anna.poser@uni-rostock.de

check for updates

Abstract: Atmospheres regulate the planetary heat loss and therefore influence planetary thermal evolution. Uncertainty in a giant planet's thermal state contributes to the uncertainty in the inferred abundance of heavy elements it contains. Within an analytic atmosphere model, we here investigate the influence that different cloud opacities and cloud depths can have on the metallicity of irradiated extrasolar gas giants, which is inferred from interior models. In this work, the link between inferred metallicity and assumed cloud properties is the thermal profile of atmosphere and interior. Therefore, we perform coupled atmosphere, interior, and evolution calculations. The atmosphere model includes clouds in a much simplified manner; it includes long-wave absorption but neglects shortwave scattering. Within that model, we show that optically thick, high clouds have negligible influence, whereas deep-seated, optically very thick clouds can lead to warmer deep tropospheres and therefore higher bulk heavy element mass estimates. For the young hot Jupiter WASP-10b, we find a possible enhancement in inferred metallicity of up to 10% due to possible silicate clouds at ∼0.3 bar. For WASP-39b, whose observationally derived metallicity is higher than predicted by cloudless models, we find an enhancement by at most 50%. However, further work on cloud properties and their self-consistent coupling to the atmospheric structure is needed in order to reduce uncertainties in the choice of model parameter values, in particular of cloud opacities.

Keywords: extrasolar planets: hot Jupiters; atmospheres; clouds; individuals: WASP-10b, WASP-39b

1. Introduction

Metallicity and core mass of giant planets contain information on protostellar disks and on the process of planet formation. Therefore, planetary metallicity, or bulk heavy element mass fraction Z_p, is an important parameter. Core accretion formation models that reproduce the metallicity of the solar system giant planets [1] predict a rapid decrease of Z_p with increasing planet mass M_p, still allowing for up to 14× solar ($Z_p \sim 20\%$) for a Saturn-mass planet but for less than 3× solar ($Z_P \sim 4.5\%$) for a 2 $M_{\rm Jup}$ planet.

Recently, Wakeford et al. (2018) [2] used transmission spectra to determine the metallicity in the atmosphere of the Saturn-mass planet WASP-39b. They retrieved a high value of $\sim$100–200$\times$ solar. This is not only higher than the prediction from core accretion formation but also higher than the upper limit of 55$\times$ solar for the atmospheric metallicity as inferred from structure models for this planet [3]. Moreover, for some massive giant planets such as the 3 M_{Jup} planet WASP-10b [4], structure models predict a significant heavy element enrichment of Z_p of 10% or more [5].

In this paper, we pursue the possibility of uncertainty in the planet's inferred bulk metallicity due to an additional opacity source of limited vertical extent. We call it a cloud layer; however, we do not model any physical aspect of real clouds except the potential additional longwave opacity. Because of their optical properties, clouds in the atmosphere are known to modify the observable transmission spectrum [6] and the temperature structure of the atmosphere itself [7]. Clouds also influence the atmospheric scale height, which provides a direct link to the mean molecular weight of the atmosphere [8]. Since the latter depends on atmospheric metallicity, its value can be inferred from the observed transmission spectrum in combination with radiative transfer calculations, which yield the scale heights of the observed portion of the atmosphere. In this work, we follow a different approach—inferring the atmospheric metallicity from planetary structure models that are primarily constrained by the observed mass, radius, and age of the star as explained below. In gaseous planets, the radiative atmosphere transitions smoothly into the adiabatic deep interior. The pressure—temperature (P–T) conditions at this transition influence the internal temperatures and the possible intrinsic heat loss [9]. Higher temperatures at a given pressure level in a fluid planet lead to lower densities and to expansion if not compensated for by an increase in heavy element abundance, an effect that is still relevant for the ice giants Uranus and Neptune [10]. Therefore, atmospheric temperature profile and our inference of a planet's metallicity are strongly coupled. We include a cloud layer into our coupled planetary atmosphere, interior, and evolution calculations by using the semi-analytic model of Heng et al. (2012) [11], which allows us to conveniently investigate the influence of assumed cloud opacity and assumed cloud pressure level on the atmospheric P–T profile. This model is applied to the two giant planets: WASP-10b and WASP-39b. Both planets may harbor clouds since their atmospheric P–T profiles intersect with a number of condensible species, as shown in Figure 1.

Candidates of cloud forming species for these planets are Na_2S, MnS, Cr, and silicates. This study is not the first one to investigate the influence of cloudy and cloud-free atmospheres on the evolution of gaseous planets. Clouds have been considered in models for planets with hydrogen-dominated atmosphere before. For instance, Linder et al. (2018) [12] studied the influence on the spectra and thermal evolution of weakly irradiated exoplanets while Kurosaki et al. (2017) [13] studied the influence of water clouds on the cooling of the ice giant Uranus. For strongly irradiated hot Jupiters, Barman et al. (2001) [14] find a large heating effect in the upper atmosphere from reflection of stellar incident flux and absorption of dust grains at infrared wavelengths in comparison to clear atmospheres, with consequences on the emergent spectra, while Baraffe et al. (2003) [15] find a minor influence of dusty versus clear irradiated atmospheres for the luminosity evolution of hot Jupiters.
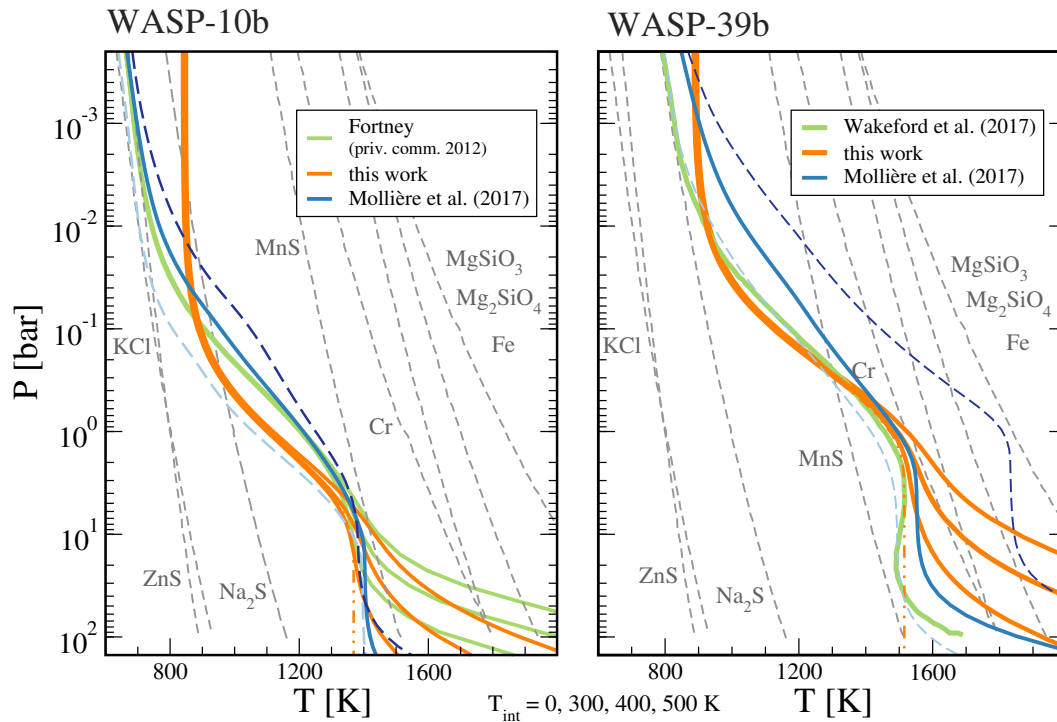
Figure 1. Condensation curves (grey dashed) of some species as labeled for solar-metallicity atmospheres (taken from Ref. [16]) and cloud-free *P–T* profiles (solid) for WASP-10b (left) and WASP-39b (right). Intersection points are possible cloud forming pressure levels. Orange *P–T* profiles are our fits to the profiles for WASP-10b from J. Fortney (pers. comm. 2012) as well as our fit to the global average profile of Wakeford et al. [2] for WASP-39b for different T_{int} values. Additionally, we show the obtained clear profiles by Mollière et al. [17] for their deduced atmospheric enrichment in [Fe/H] (solid blue) and $10\times$ smaller vs. larger enrichment (dashed light blue vs. dashed dark blue).

In Section 2, we list the relevant observed system parameters and describe our modeling approach for the atmosphere with a cloud layer, the interior, and the thermal evolution. Results for WASP-10b are presented in Section 3 and for WASP-39b in Section 4. In particular, we take the Z_p value of Thorngren and Fortney (2019) [3] for WASP-39b as an input parameter for our models and see if the high predicted atmospheric metallicity of Wakeford et al. (2018) [2] can be reached just by including an additional opacity source which may mimic the effect of a cloud deck. We compare the obtained atmospheric models with self-consistent clear and cloudy models by Molliére et al. (2017) [17] in Section 5. A summary is given in Section 6.

2. Methods

2.1. Planet and Star Parameters

WASP-10b is a massive (2.96 M_{Jup}) and non-inflated ($T_{eq} = 950$ K) hot Jupiter. Its young age of 270 ± 80 Myr [18–20] makes it an interesting object to study planet formation and evolution. While early radius estimates predicted a rather large radius of $\sim 1.27\,R_{Jup}$ [19], subsequent careful analysis of the spots on the K5 dwarf host star suggested a 20% smaller planet radius of 1.02 R_{Jup} [4], which we use in this study.

WASP-39b is a Saturn-mass planet (0.28 M_{Jup}) with a large radius (1.27 R_{Jup}) and therefore low density $\rho = 0.141\,\rho_{Jup}$ [21]. It is orbiting a late G-type star, which is smaller and, with an age of 9^{+3}_{-4} Gyr, possibly older than the Sun. The observational parameters used here for WASP-10b and WASP-39b are listed in Table 1.

Table 1. Stellar and planetary parameters.

	WASP-10b	WASP-39b [5]
M_P	$2.96^{+0.22}_{-0.17}\,M_{\mathrm{Jup}}$ [1]	$0.28 \pm 0.03\,M_{\mathrm{Jup}}$
R_P	$1.03^{+0.077}_{-0.03}\,R_{\mathrm{Jup}}$ [4]	$1.27 \pm 0.04\,R_{\mathrm{Jup}}$
a	$0.0369^{+0.0012}_{-0.0014}\,\mathrm{AU}$ [1]	$0.0486 \pm 0.0005\,\mathrm{AU}$
e	0.013 ± 0.063 [3]	0
$T_{\mathrm{eq,A=0}}$	$950^{+30}_{-26}\,\mathrm{K}$ [4]	$1116^{+33}_{-32}\,\mathrm{K}$
P	3.09 d	4.05 d
$M_\star$	$0.75\,M_{\mathrm{Sun}}$ [2]	$0.93 \pm 0.03\,M_{\mathrm{Sun}}$
$R_\star$	$0.67\,R_{\mathrm{Sun}}$ [4]	$0.895 \pm 0.023\,R_{\mathrm{Sun}}$
$T_\star$	$4675 \pm 100\,\mathrm{K}$ [1]	$5400 \pm 150\,\mathrm{K}$
age $\tau_\star$	$270 \pm 80\,\mathrm{Myr}$ [3]	$9^{+3}_{-4}\,\mathrm{Gyr}$

[1] Ref. [19], [2] Ref. [18], [3] Ref. [20], [4] Ref. [4], [5] Ref. [21].

Since we are interested in the effect of clouds relative to cloudless atmospheres on the inferred planet metallicity, we compute here planet models for a variety of cloud parameters but do not account for the observational uncertainties in planet mass and radius. The only exception is thermal evolution calculations for WASP-39b, where we request its radius at present time to drop below the 1σ upper limit.

2.2. Interior

To estimate the present structure of the planets, we connect the atmosphere to the interior and perform thermal evolution calculations. For the interior, we assume a three-layer structure of rocky core, an adiabatic, convective envelope, and a radiative atmosphere. Atmosphere and envelope consist of a mixture of hydrogen, helium and metals. Respective equations of state (EOS) are combined via the linear mixing rule. By heavy elements or metals, we denote all elements or molecules heavier than helium. Z_{atm} and Z_{env} are the heavy element mass fractions in the atmosphere and envelope, respectively, which we assume to be equal, $Z_{\mathrm{atm}} = Z_{\mathrm{env}} = Z$. This is an assumption, not ruling out other relations between atmospheric and envelope abundances [17,22]. The planetary bulk heavy element mass fraction is $Z_P = Z_{\mathrm{env}} M_{\mathrm{env}} / M_P + M_{\mathrm{core}} / M_P$, and M_{env} and M_{core} are the masses of envelope and core. For the solar reference metallicity we use $Z_\odot = 1.5\%$ [23]. For WASP-10b, we set $Z = Z_\odot$ and allow only the core mass to vary while, for WASP-39b, we allow also Z to vary. The helium to hydrogen mass fraction is set to the protosolar value of $Y = 0.27$, where $Y = M_{\mathrm{He}} / (M_{\mathrm{He}} + M_{\mathrm{H}})$. For hydrogen and helium, we use the SCvH EOS [24]. Metals in the envelope are represented by that He-EOS scaled in density by a factor of four, or by the ice EOS presented in [25]. The rocky core obeys the pressure–density relation given in [25]. The density $\rho(P,T)$ is obtained from the linearly mixed EOS at the pressure P and temperate T by interpolation. We obtain the mixed EOS by adding heavy elements to the interior and the atmosphere via the linear mixing rule $\rho^{-1}(P,T) = \sum_i X_i / \rho_i(P,T)$, where X_i denotes the mass fraction of component i and $X_{\mathrm{H}} := X$, $X_{\mathrm{He}} := Y$, $X_Z := Z$ [26]. The density profile follows a pre-computed P–T profile along the adiabat of the envelope. Increasing the temperature at fixed pressure usually decreases the density. Lower densities in the mantle result in a larger core mass to conserve the given planet mass. This is why the P–T profile is so important. Otherwise, we rely on the usual structure equations for non-rotating, spherical giant planets as previously done in [26,27].

2.3. Atmosphere Model with Clouds

The atmosphere model yields the atmospheric P–T profile. We use the 1D, plane-parallel, analytical atmosphere model by Heng et al. (2012) [11] for hot Jupiters. It is based on the two-stream solution and dual band approximation, where the incoming and outgoing radiation fluxes are described by different frequency-averaged mean opacities. The incoming flux is represented by the short-wave opacity κ_S, equivalent to the opacity κ_{vis} for visual light used in [28], while the

outgoing flux is described by the long-wave opacity κ_L equivalent to κ_{th} in [28] for thermal radiation. Following Heng et al. [11], κ_S is constant with respect to temperature and pressure while κ_L may have a dependence on pressure. Indeed, gas opacities significantly depend on pressure because of pressure broadening or collision induced absorption. Cloud decks are included as an additional opacity source $\kappa_c(P)$ to the constant long-wave opacity $\kappa_{L,0}$ of the otherwise cloudless atmosphere,

$$\kappa_L(P) = \kappa_{L,0} + \kappa_c(P) . \tag{1}$$

The analytic model atmosphere provides a relation between global mean temperature T and longwave optical depth $d\tau_L = \kappa_L dm$, where m is column mass from top to bottom, as well as the parameter $\tau = \kappa_L m$. We call the latter here optical depth although this holds only if $\kappa_L = $ const.. The T–τ relation makes use of the Eddington coefficients $\mathcal{E}_1 = 1/3$ and $\mathcal{E}_2 = 1/2$ to close the set of equations for the moments of radiation transfer. It reads (cf. Equation (31) in [11])

$$T^4 = \frac{T_{\text{int}}^4}{4} \left(2 + 3 \int_0^m \kappa_L dm' \right) + \frac{T_{\text{eq}}^4}{2} \left[1 + \frac{\gamma}{\sqrt{\xi}} E_2 \left(\frac{\kappa_S m'}{\sqrt{\xi}} \right) + 3 \int_0^m \kappa_L E_3 \left(\frac{\kappa_S m'}{\sqrt{\xi}} \right) dm' \right] , \tag{2}$$

with $E_j(x) = \int_1^\infty y^{-j} \exp(-xy) \, dy$ as the exponential integrals. Equation (2) depends on the cloud opacity through κ_L and the opacity ratio $\gamma = \kappa_S/\kappa_L$. Furthermore, the global mean temperature T depends on the intrinsic heat flux $F_{\text{int}} = \sigma_B T_{\text{int}}^4$, which is the outgoing flux from the planet at the bottom of the atmosphere, and on the zero-albedo irradiation flux $\sigma_B T_{\text{eq},0}^4 = \sigma_B T_\star^4 (R_\star/2a)^2$ where σ_B is the Stephan–Boltzmann constant. Thus, $(1-A)^{1/4} T_{\text{eq},0}$ is the globally averaged temperature a planet of albedo A would adopt if in radiation equilibrium with the incident flux. Since a scattering parameter $\xi < 1$ would be inconsistent with a non-uniform opacity, here $\kappa_L(P)$, we set $\xi = 1$ (no scattering) and take scattering into account only via the albedo in T_{eq}, which we set to $A_B = 0.3$ [29,30], while noting that other work suggests smaller values (e.g., [31]). More recently, the geometric albedo of several exoplanets has been derived from secondary eclipse data and found to be quite small, even less than 0.1 [32]. On the other hand, the Bond albedo value of Jupiter itself has recently been revised upward from its Voyager-data based value of 0.34 to the new Cassini-data based value of 0.5 [33]. To study the thermal evolution of irradiated giant planets as a function of uncertainty in albedo is left to future work. For a more consistent treatment of scattering in the presence of non-uniform absorption, see Ref. [34]. For the cloud-free ($\kappa_L = \kappa_{L,0}$) atmosphere without scattering ($\xi=1$), Equation (2) reduces to the global average temperature profile of Guillot (2010) [28]. The P–τ relation for constant gravity g and pressure-dependent longwave opacity reads

$$P = m \cdot g = (\tau/\kappa_L) \, g . \tag{3}$$

We use the cloud-free model to constrain the parameter γ. For WASP-10b, we fit to 1D, non-gray, atmospheric P–T profiles specifically calculated for this planet for different values of T_{int} [35] (see Figure 1). For WASP-39b, we fit κ_S and $\kappa_{L,0}$ to the global averaged P–T profile from Ref. [16] for a $1\times$ solar composition metallicity. We find $\kappa_{L,0} = 0.0136$ cm^2/g, $\kappa_S = 0.002$ cm^2/g ($\gamma = 0.147$) for WASP-10b and $\kappa_{L,0} = 0.006$ cm^2/g, $\kappa_S = 0.00037$ cm^2/g ($\gamma = 0.062$) for WASP-39b. However, albeit using solar-composition models to fit our double-gray clear atmosphere, it is important to notice that an increase (or decrease) of atmospheric enrichment changes the position of the isotherm [36,37]. An increase in atmospheric metallicity leads to higher temperatures in the isothermal part of the atmosphere [38]. In the case of WASP-39b, where possibly the atmosphere is enriched by a factor of 100–200$\times$ solar value, the isotherm would be pushed to even hotter temperatures.

The results of these fits are shown in Figure 1. In Figure 2, we show the Rosseland mean opacities along the P–T profiles for the present planets using the fit formula of Valencia et al. [39] to the tabulated values of Freedman et al. [40]. We conclude that our obtained long-wave opacity values $\kappa_{L,0} \sim 0.01$ cgs are appropriate mean Rosseland mean opacities in the radiative atmospheres of both planets.
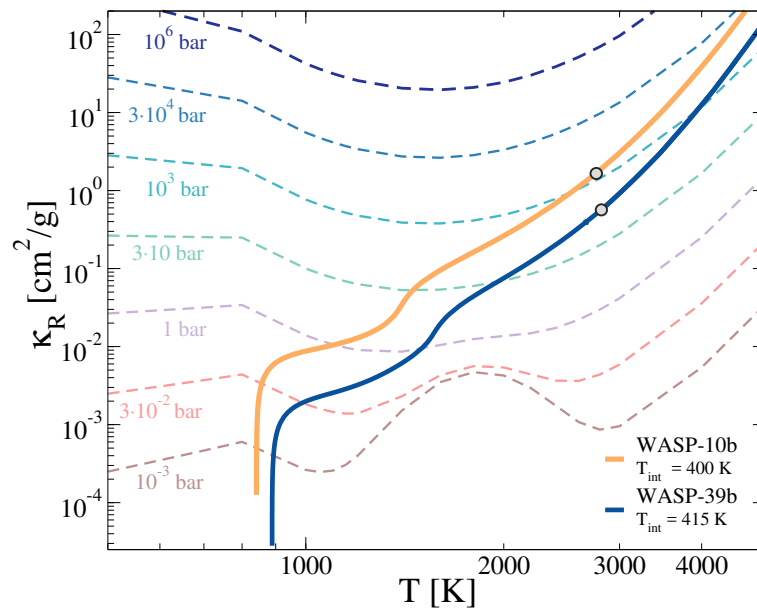
Figure 2. Fit of Valencia et al. [39] to the Rosseland mean opacities κ_R of Freedman et al. [40] along isobars (dashed) and κ_R along the present *P–T* profiles for WASP-10b (solid orange) and WASP-39b (solid blue). The transition from the atmosphere to the interior is marked by grey circles.

2.4. Cloud Model

The model of Heng et al. [11] for a purely absorbing cloud provides a simple toy model approach that reduces the complexity of the problem to few parameters while including the important greenhouse effect of clouds. The cloud opacity can be assumed to take the shape

$$\kappa_c(P) = \kappa_{c_0} \exp\left[-\Delta_c \left(1 - P/P_c\right)^2\right] \quad . \tag{4}$$

The cloud opacity depends on the normalization factor κ_{c_0}, the location of the cloud deck P_c, and the cloud deck thickness parameter Δ_c, where small Δ_c values yield vertically extended cloud decks while large Δ_c values lead to thin cloud decks. By construction, the cloud opacity adopts a Gaussian shape. The cloud optical depth τ_c adds to the longwave optical depth τ_L. This is illustrated in Figures 3 and 4 for WASP-10b and WASP-39b, respectively, for cloud parameters considered in this work. The cloud normalization opacity κ_{c_0} was adjusted to reach optical depth values τ_L as in [7,41].

In this cloud model, cloud decks lead to warming of the atmosphere above the cloud, although high above the cloud deck the effect may reverse and lead to cooling (not shown in Figures 3 and 4). Nevertheless, the enhancement of opacity and optical depth in a limited region of the atmosphere leads to a strong heating of the deep atmosphere (left panel) and the typical isothermal region of temperature T_{iso}, which is most clearly seen for $T_{\text{int}} = 0$, is shifted toward higher T_{iso} values. For $T_{\text{int}} = 0$, the isothermal region extends all the way down to the center of the planet. Of interest to this study is the question of how much the warming effect of the clouds affects the deep interior of planets of finite intrinsic heat fluxes ($T_{\text{int}} > 0$), and how much this warming effect affects our inferred heavy element abundances.
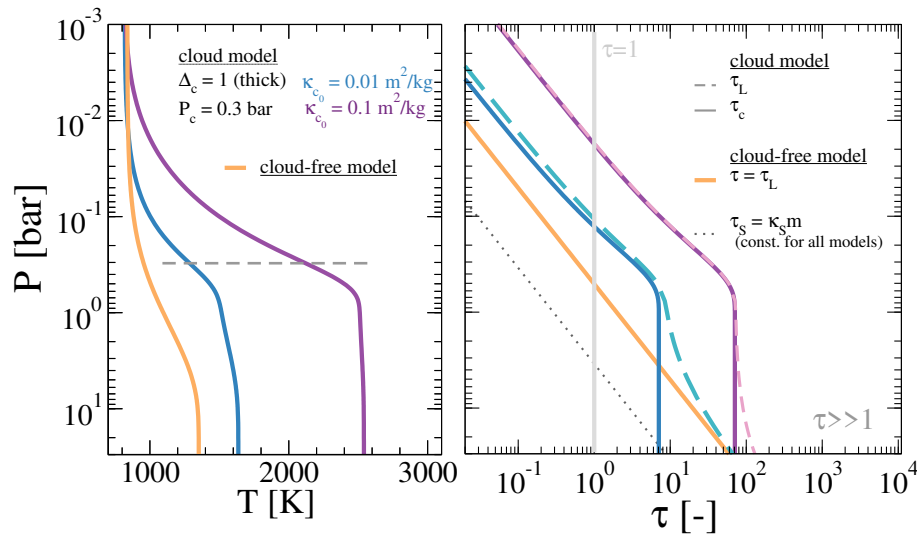
Figure 3. Influence of two cloud decks (optically thin, blue; optically thick, violet, cloud-free, orange) on the *P–T* relation of WASP-10b for $T_{int} = 0$ K (left) and *P–τ*-relation (right) for optical depth τ_L (dashed) and cloud optical depth τ_c (solid), which contributes to τ_L (cf. Equation (49) in [11]). The cloud decks are located at 0.3 bar and are of vertical extension $\Delta_c = 1$.
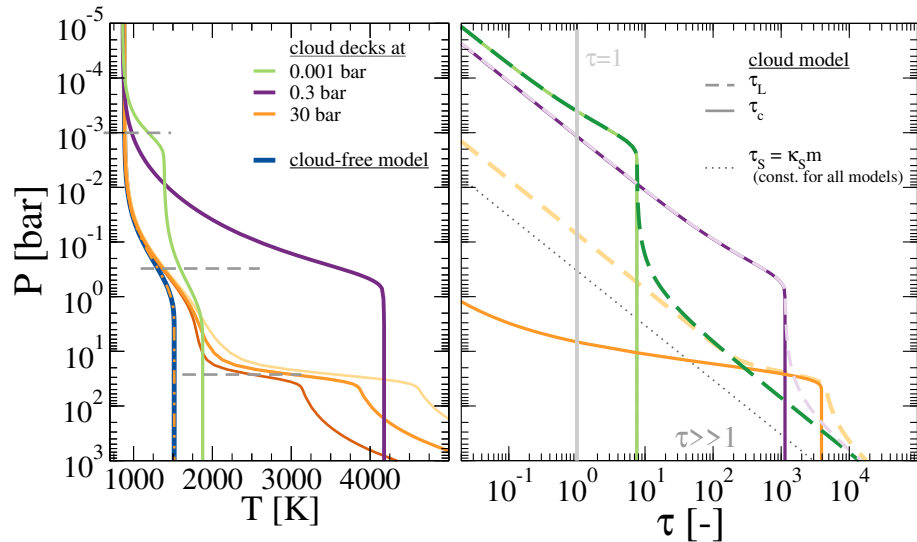
Figure 4. Similar to Figure 3 but for WASP-39b and three possible cloud locations at 0.001 (green), 0.3 (purple) and 30 bar (orange) as well as the cloud-free atmosphere (blue, only left panel). For the cloud deck at 30 bar, we show the resulting *P–T* profiles for $T_{int} = 300, 400, 500$ K (from darker to lighter orange) as well as the isotherm (dash-dotted, orange).

To address this question, we investigate six different possible cloud layers for WASP-10b and three for WASP-39b. They are selected based on the condensation curves of typical cloud species [16,42,43] shown in Figure 1. Possible cloud forming species and their approximate intersection pressures are listed in Table 2. We take those pressures as the cloud deck mean location P_c in Equation (4). We consider optically thick ($\kappa_{c_0} \sim 10 \, \kappa_{L,0}$, $\tau_c > 1$, see Figures 3 and 4) and optically very thick ($\kappa_{c_0} \sim 100 \, \kappa_{L,0}$, $\tau_c > 10$) cloud decks. However, for simplicity, we label them *optically thin* and *optically thick*, respectively. The vertical extension is set to $\Delta_c = 1$ where possible in order to allow for a non-zero (Δ_c sufficiently large) but not tremendously too strong (Δ_c sufficiently small) effect. In the real planet, several cloud decks may be present simultaneously and they may be patchy, while, in this model, only one permanent cloud deck is considered and assumed to be uniform.

Table 2. Cloud deck parameters considered in this work.

	Cloud Species	P_c [bar]	Δ_c [-]	κ_{c_0} [m^2/kg]
WASP-10b	KCl/ZnS	0.01	1	0.01
	KCl/ZnS	0.01	1	0.1
	Na$_2$S	0.3	1	0.01
	Na$_2$S	0.3	1	0.1
	MnS	10	10	0.01
	MnS	10	10	0.1
WASP-39b	Na$_2$S	0.001	1	0.2
	MnS	0.3	1	0.1
	MgSiO$_3$/Cr	30	10	0.01

2.5. Atmosphere-Interior Connection

The transition to the adiabatic interior is made where the local numeric temperature gradient $\nabla_{T,local}$ is larger than the adiabatic gradient ∇_{ad} taken from the EOS table. Further, we see a convective region forming in most cloudy models above the cloud deck. As the starting point for the adiabatic interior we take the lower intersection of $\nabla_{T,local}$ with ∇_{ad}. Generally, the boundary moves to lower pressures with increasing T_{int} and T_{eq} [9].

2.6. Planetary Evolution

To determine the present T_{int} value of a planet, we perform thermal evolution calculations. The planets are assumed to be of the same age as the parent star within an uncertainty of a few Myr. Further, we assume an orbital location constant in time. Of course, the planets once migrated to their present location, but this is thought to have happened on a comparably short timescale during the first 10 Myr [44]. Integrating the energy balance equation over time, we obtain the evolution of luminosity L and radius $R_P(t)$

$$L_{eff} - L_{eq} = L_{int} = L_{sec} + L_{radio} + L_{extra} \tag{5}$$

with $L_{eq} = 4\pi R_P^2 \sigma_B T_{eq}^4$ being the absorbed and re-emitted flux. The heat loss from the interior $L_{int} = 4\pi R_P^2 \sigma_B T_{int}^4$ contains three further components. $L_{sec} = -4\pi R_P^2 \int_0^M dm T(m) \frac{ds}{dt}$ accounts for cooling and contraction of the planet, L_{radio} stands for radiogenic heating, but is of minor importance for H/He-dominated gas giants, and $L_{extra} = \epsilon 4\pi R_P^2 \sigma_B T_{eq}^4$ denotes an extra energy that may be needed to inflate the planet. In Ref. [45], the statistically most likely values of ϵ as a function of irradiation flux are determined for a sample of planets that exclude planets with $M_P < 0.5\,M_{Jup}$. Here, we need the extra heating term in order to reach the large age of the 0.28 M_{Jup} planet WASP-39b. Depending on the distribution of heavy elements in the envelope vs. core, we find ϵ = 2.75–4.00% compared to the majority of hot Jupiters where ϵ = 1–3% [45]. In Figure 5, we show the radius evolution of WASP-39b with and without extra heating. For the young WASP-10b, we do not need extra heating to explain its measured radius.
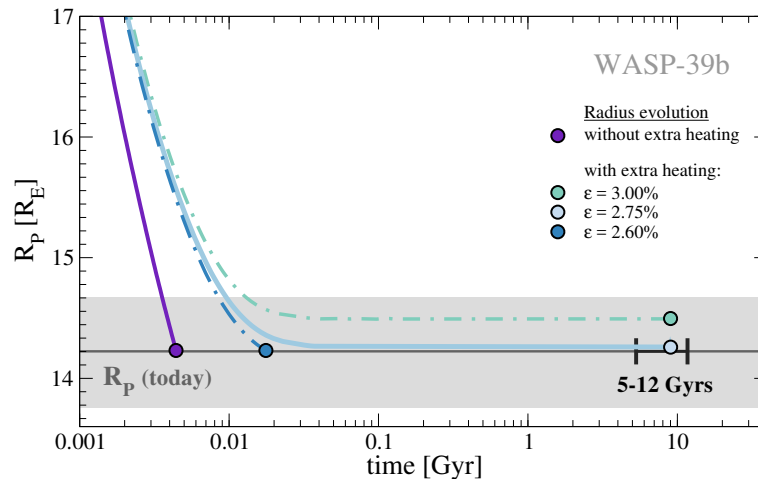
Figure 5. Radius evolution for WASP-39b with (bluish) and without (purple) extra heating. The planet stays hot and inflated for several Gyrs as the additional heating ϵ prevents further contraction.

3. Results for WASP-10b

In Figure 6, we show atmospheric P–T profiles for WASP-10b for finite T_{int} values for a cloud deck at 0.3 bar and two different cloud opacities $\kappa_c = 0.01$ and 0.1 m^2/kg.

As shown in Figure 3 for $T_{int} = 0$ K, clouds can shift the temperature in the isothermal region significantly toward higher values. This is also the case for finite T_{int} values. Figure 6 also shows that clouds shift the onset of the adiabatic interior to deeper regions. Both effects become more pronounced with increasing cloud opacity. However, we find that the interior adiabat follows the adiabat of the cloud-free case of same T_{int} value.
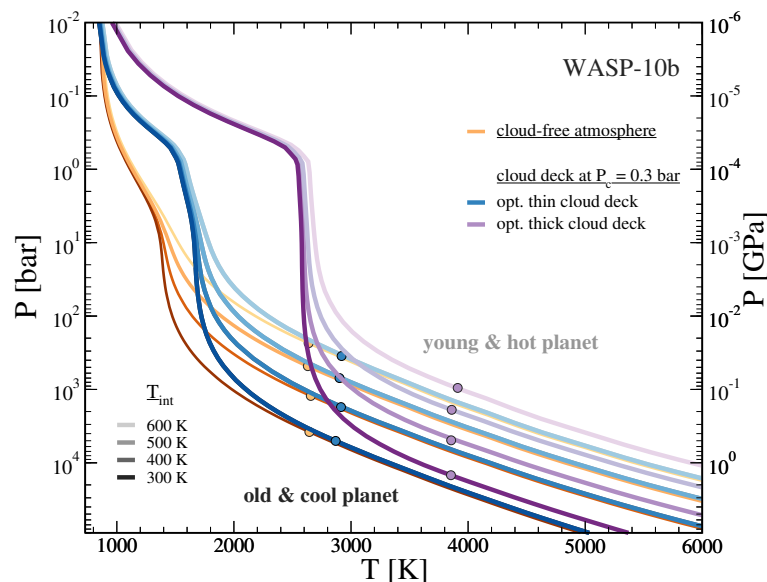
Figure 6. Atmospheric P–T profiles of WASP-10b for finite T_{int} values of 300, 400, 500, and 600 K (from bottom to top) and three cloud deck scenarios: optically thin at 0.3 bar (blue), optically thick at 0.3 bar (purple), and cloud-free (orange). Circles mark the transition between atmosphere and adiabatic interior.

The optically thin cloud (blue) in Figure 6 shifts T_{iso} by about 400 K from ~1400 K to ~1800 K. Under these conditions, the initially assumed Na$_2$S molecules would no longer condense while silicate clouds (Mg$_2$SiO$_3$ and Mg$_2$SiO$_4$) might form in present WASP-10b. In this sense, we consider the optically thin cloud at 0.3 bar a more likely option for WASP-10b. On the other hand, the assumption of

the optically thick cloud at 0.3 bar (purple) clearly shifts T_{iso} far beyond any temperature regime where heavy elements might condense out. Similar reasoning applies to the four other cloud cases considered for WASP-10b. Our optically thick clouds cause too strong heating, evaporating any clouds, while in the atmosphere heated by the optically thin clouds condensible species could still condense out. This is the picture that emerges if using condensation curves for solar-metallicity atmospheres. Despite the apparent inconsistencies with the optically thick clouds, we keep them in the loop. This allows us to place an upper limit on the quantitative influence of assumed long-wave absorbers on the inferred metallicity.

We proceed with the case of the cloud at 0.3 bar and show the radius evolution in Figure 7.

Cooling times in agreement with the known age of the system can easily be obtained for all considered cloud models. Lower assumed T_{int} values for the present planet lead to longer cooling times. We find that optically thick clouds with their strong heating effect slow down the heat loss from the interior, leading to higher T_{int} values. They also slow down the contraction of the planet. To obtain a radius for the present planet in agreement with the known age and radius, the planet with optically very thick clouds must harbor a larger amount of heavy elements. That leads to the link between M_{core} in representation of planetary bulk heavy element mass Z_P and $T_{\text{int}}(t_0)$ shown in Figure 8. Thick lines in Figure 8 show the models matching R_P, M_P and the error range of the age of the system.

The higher is T_{iso}, rising with the optical thickness and P_c, the larger is the core mass. The more likely option of the optically thin cloud deck at 0.3 bar (solid dark blue) leads to a 10% higher core mass compared to the cloud-free model (orange). For optically thin clouds high in the atmosphere, the heating effect on the atmosphere is lower and the influence on inferred metallicity is negligible (the blue-dashed curve in Figure 8 coincides with the orange curve). For the optically thin clouds deep in the atmosphere the heating effect is strong and therefore we had to make the cloud more tenuous by increasing Δ_c instead. The maximum enhancement in inferred heavy element abundance is about 10% and well represented by the medium-height cloud at 0.3 bar. For optically thick clouds, which are not likely options, we obtain a maximum increase in inferred heavy element content of up to 100%.
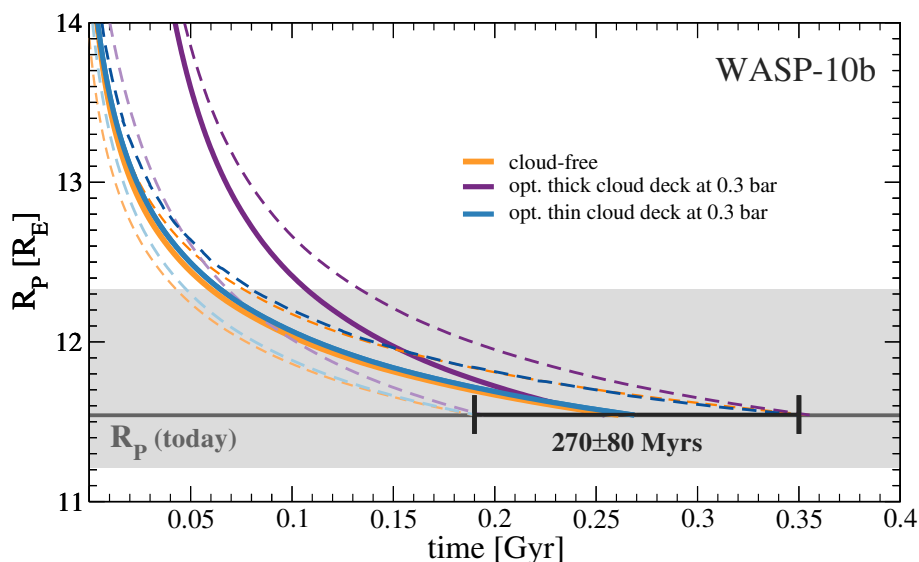
Figure 7. Radius evolution of WASP-10b for the cloud-free atmosphere (orange) as well as for optical thick (purple) and optical thin (blue) clouds decks at $P_c = 0.3$ bar. Solid lines yield a cooling time of 270 Myr while dashed lines within the 1σ uncertainty of the age, e.g., light dashed lines then describe models reaching the lower limit of the age constraint of 190 Myr.

Thorngren and Fortney (2019) find for WASP-10b $Z_P = 0.12 \pm 0.02$, using $M_P = 3.15\,M_{\text{Jup}}$ and $R_P = 1.08\,R_{\text{Jup}}$, in agreement with our results for the cloud-free model, where we obtain $Z_P = 0.13$ at $T_{\text{int}} = 400$ K.
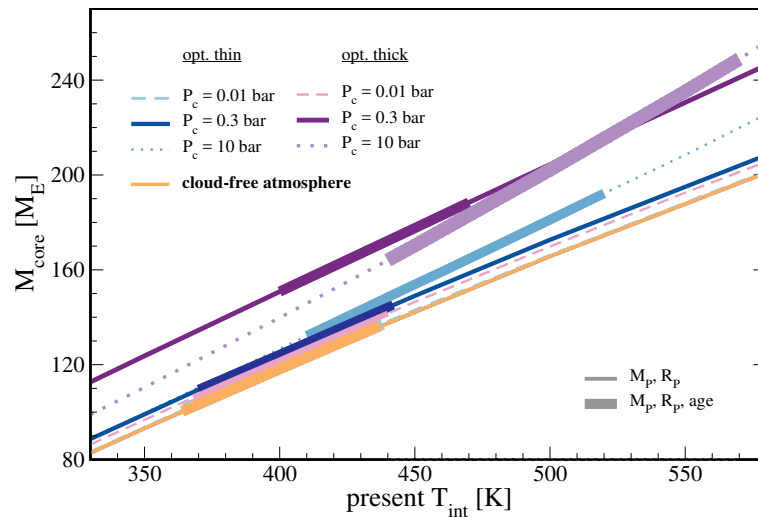
Figure 8. M_{core}-T_{int} relation for WASP-10b assuming cloud-free atmosphere (orange) and six different cloud decks in the atmosphere. Thin lines indicate the results obtained by M_P, R_P, thick bars highlight the solutions that also satisfy the age constraint.

4. Results for WASP-39b

4.1. Cloud Height

In Figure 9, we show the atmospheric P–T profiles for WASP-39b with and without cloud decks. We find that the high cloud deck at 0.001 bar would heat the upper atmosphere so much that only silicates could condense out at such low pressures.
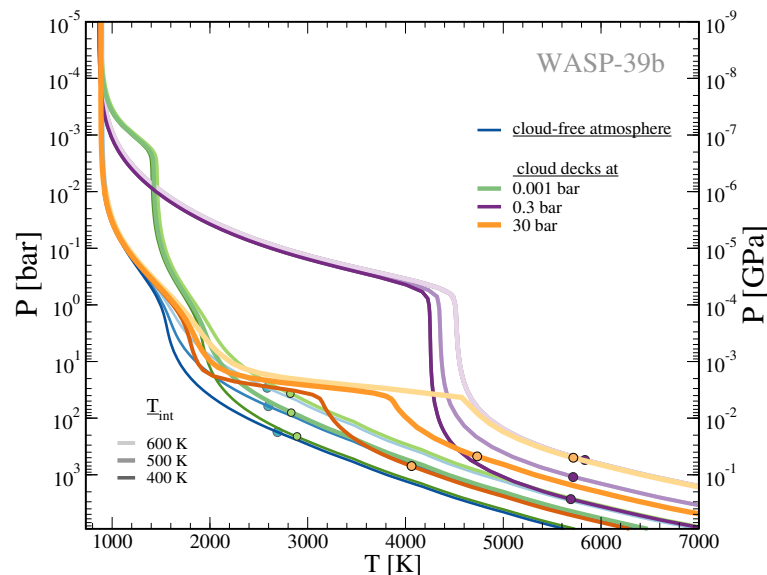
Figure 9. Atmospheric P–T profiles of WASP-39b for finite T_{int} values of 400, 500, and 600 K for three decks located at 0.001 (green), 0.3 (purple), and 30 (orange) bar as well as the cloud-free atmosphere (blue). Circles mark the transition between atmosphere and adiabatic interior.

The analysis in Ref. [2] indicates the presence of clouds on only one side of the limb while a clear sky on the other. In their 3D global circulation models, a high-metallicity atmosphere was clearly required to explain the spectra while optically thick, uniform clouds would not much influence the fit. Thus, the observations do not well constrain the presence of clouds, in particular in the deep atmosphere below ∼0.1 bar or deeper. We proceed with the cloud deck at 30 bar. According to Figures 1 and 9, this cloud deck could be a more likely solution for the 10–30 bar region while the heating of the

deeper troposphere for the deep-seated cloud at 30 bar is very strong. At 3000–4000 K, condensible species will not condense out. On the other hand, a uniform silicate cloud layer at 30 bar may impose a compositional gradient, which itself may inhibit convection unless the super-adiabaticity becomes sufficiently strong. As a result, the temperature gradient needed to transport the internal heat outward must be larger than in the adiabatic case without cloud. For the solar system giant planets, this effect may amount up to several 100 Kelvins [46]. Therefore, we consider the deep, optically thin cloud at 30 bar a possible option for WASP-39b. We caution that a number of further effects may lead to a more complex picture than drawn here. Condensation of heavier species decreases the mean molecular weight of the surrounding medium and condensates may decouple from the gas phase, affecting the density difference between vertically moving parcels and the background state and thus the possible stability. Moreover, since the Rosseland mean opacity depends on metallicity [40], redistribution of condensible species by condensation also influences the radiative gradient of the background state. Leconte et al. (2017) [46] also found that possible stability requires a sufficiently high mixing ratio of condensible species. Whether sufficient conditions for stability are satisfied in the atmospheres of the hot Jupiters remains to be investigated.
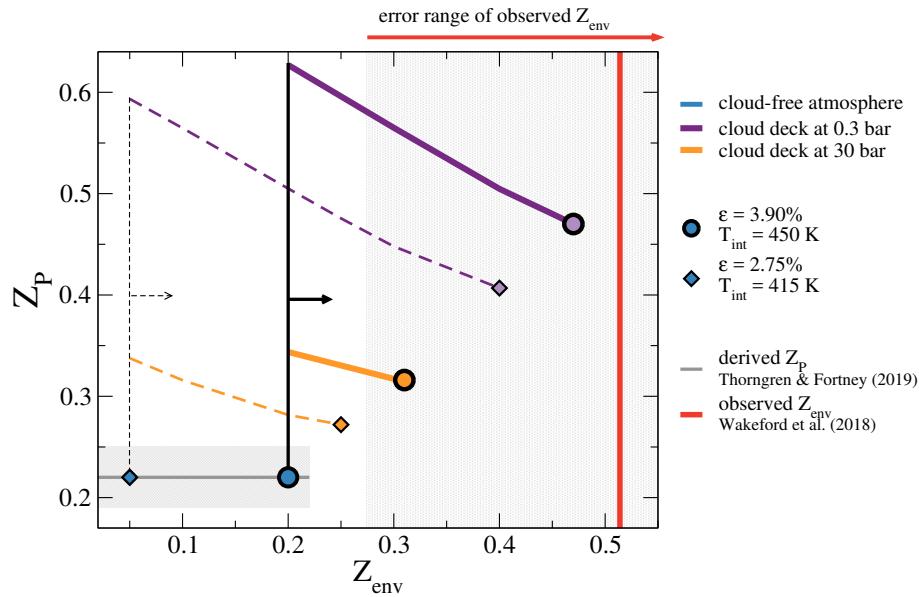
4.2. Metallicity

WASP-39b is an interesting planet because of its observationally determined atmospheric water abundance. Recently, Wakeford et al. (2018) completed the existing transmission spectrum data in the optical obtained with HST STIS [47] and VLT FORS2 [48] and in the infrared obtained with *Spitzer* IRAC [47] by adding spectral data in the near infrared using the HST WFC3 camera. The clearly detected water absorption features allowed them to retrieve the atmospheric metallicity, temperature, and cloudiness of the observationally accessible part of the atmosphere amongst other parameters. Combined likelihood analysis of their isothermal equilibrium model yielded a high-metallicity atmosphere of $\sim151^{+48}_{-46}\times$ solar abundances, though their free-chemistry model yielded a lower metallicity of $\sim117^{+14}_{-30}\times$ solar abundances.

The high metallicity of 100–200$\times$ solar corresponds to a heavy element mass fraction $Z_{\text{env}} \sim$ 0.25–0.75 (see Table 3). Cloud-free structure model of WASP-39b yield a maximum Z_p value of 0.25 [3], where $Z_p \geq Z_{\text{env}}$ due to the possible presence of a core.

First, we require our cloud-free models to have $Z_P = 0.22 \pm 0.03$ as found in Ref. [3] for cloud-free models. Because this planet seems to be inflated (see Section 2.6), we account for extra heating $\epsilon > 0$. For $Z_{\text{env}} = 0.05$, we find $\epsilon \approx 2.75\%$, whereas for $Z_{\text{env}} = 0.2$ we find $\epsilon \approx 3.90\%$. These ϵ values are then used also for the models with clouds. From our experience with the models for WASP-10b, where optically thin clouds have a minor effect on T_{int}, we also use the same range of T_{int} values as found for the cloud-free case, so that no additional evolution calculations are necessary. Figure 10 shows the results on Z_{env} and Z_p. Even for the extreme case of the optically thick cloud, high atmospheric metallicities of $Z_{\text{env}} \sim 0.5$ as observationally derived can barely be reached. Interestingly, however, for the optically thin deep cloud the enhancement in inferred metallicity amounts to about 50%, which allows us to obtain solutions just within the observational uncertainty of Wakeford et al. [2]. A summary of the metallicities for WASP-39b is given in Table 3.

With our favored cloud model for WASP-39b, the optically thin deep cloud, we obtain a maximum envelope metallicity of 0.3, which is 50% higher than our value in the cloud-free case. However, the maximum Z_{env} value still falls short of the observed value. Our results therefore confirm the conclusion of Thorngren and Fortney (2019) of additional sources of uncertainty relevant to WASP-39b. One source of uncertainty is the EOS. While the H/He-EOS was found to induce an uncertainty of a few percent only for massive hot Jupiters and brown dwarfs, wherein matter is largely degenerate [49], this effect might be stronger for warm, lower-mass planets where temperature effect on the P–ρ relation can be stronger. The composition of heavy elements matters as well. Icy cores typically have a 50% higher mass than rocky cores if otherwise the same modeling procedure is applied.

Figure 10. Range of envelope metallicity Z_{env} due to different atmosphere models without clouds (blue), with optically thick cloud deck at 0.3 bar (purple), and optically thin at 30 bar (favored case, orange). Circles/diamonds indicate the maximum Z_{env} value for a fully-mixed planet. The solid and dashed colored lines indicate models with different T_{int}/ϵ-values obtained for the cloud-free models. The arrows indicate the increase of Z_{env} when clouds are switched on.

Table 3. Constraints on atmospheric metallicity of WASP-39b.

WASP39-b		
Wakeford et al. (iso. eq.)	$[M/H]=151^{+48}_{-46} \times$ solar	$Z_{env} = 0.514^{+0.25}_{-0.24}$
Wakeford et al. (free-chem.)	$[M/H]=117^{+14}_{-30} \times$ solar	$Z_{env} = 0.45^{+0.09}_{-0.17}$
Thorngren and Fortney	$Z{:}H_P = 40.51 \pm 8.3 \times$ solar	$Z_P = 0.22 \pm 0.03$ (=Z_{env}, fully mixed)
This work, cloud-free		$Z_{env,max} = 0.2$
This work, 0.3 bar cloud deck		$Z_{env,max} = 0.47$
This work, 30 bar cloud deck		$Z_{env,max} = 0.31$

Notes. For conversion of [M/H] to Z, we use Equation (3) in [3] with water as heavy element. The ratio $Z{:}H_P$ is the atmosphere abundance for a fully mixed planet, as derived derived from interior models in [3], Equation (3).

Since WASP-39b is likely to be heavy element-rich, it could also be that the heavy elements are not homogeneously distributed but that their abundance increases with depth. Even slight compositional gradients can suppress convection and delay cooling. This may be the case in exoplanets [50] and in Saturn itself [51].

5. Comparison to Self-Consistent Cloud Models

Clouds will not only be important at infrared wavelengths, but they can also contribute to absorption and scattering of irradiation at short wavelengths. This is neglected in the cloud model we use. Out of the codes capable of calculating the structure of self-luminous and/or irradiated planets (e.g., [52–54]), we here compare the ad-hoc approach of Heng et al. (2012) [11] to the self-consistent atmosphere models with clouds of Mollière et al. (2017) [17], who used the *petitCODE* [37]. Within this code, models with clouds and different metallicities have been calculated specifically for WASP-10b and WASP-39b. That code calculates radiative-convective equilibrium atmospheric structures and spectra of extrasolar planets self-consistently, assuming chemical equilibrium. The radiative transfer model implements absorption, emission and scattering. It implements the Ackerman and Marley (2001) [55] cloud model for clouds composed of $MgAl_2O_4$, Mg_2SiO_4, Fe, KCl and Na_2S. Particle opacities are calculated using Mie theory (assumption of spherical, homogeneous grains) or the distribution of

hollow spheres (approximating irregularly shaped dust aggregates). For both planets, WASP-10b and WASP-39b, we plot the clear and cloudy solutions of Mollière et al. (2017) in comparison to our clear and cloudy atmosphere models for $T_{int} = 400$ K in Figure 11. Mollière et al. (2017) used cloud models which differ in the assumptions of the grain shape, the standard settling parameter f_{sed} from the Ackerman and Marley model, the maximum cloud mass fraction, the width of the cloud particle size distribution as well the inclusion of iron clouds (see Table 2 in [17]). The different model assumptions result in different atmospheric structures. For temperate giant planets, such as WASP-10b and WASP-39b, they investigated cold cloud models as well, where only Na_2S and KCl are considered as possible cloud species (Figure 11, red) as for this temperature regime higher temperature condensates may not mix up from their deep cloud deck locations.

For both planets, the cloudy atmospheric structures from Mollière et al. (2017) lead to both cooler and hotter isotherms. Their favored *cold* cloud models, only using Na_2S and KCl as cloud species, lead to cooler isotherm for all different cloudy model parameters compared to the clear atmosphere in orange. In contrast, in this work, the fit parameter of the double-gray atmosphere and the added cloud opacity lead to a warmer atmosphere beneath the cloud deck for all of our assumed cloud decks in the atmosphere. For WASP-10b, there is only one model (dashed light blue) that yields a hotter isotherm, whereas for WASP-39b there are three cloudy models that yield a hotter isotherm compared to the cloud-free case. This comparison suggest that our favored 0.3 bar cloud model for WASP-10b may be supported by the *hot* cloud model of Mollière et al. (2017), down to significant depths of ~1 kbar, while for WASP-39b our favored 30 bar cloud model is supported to ~100 bar and thus may overestimate the here obtained influence on the Z_{env} of WASP-39b.
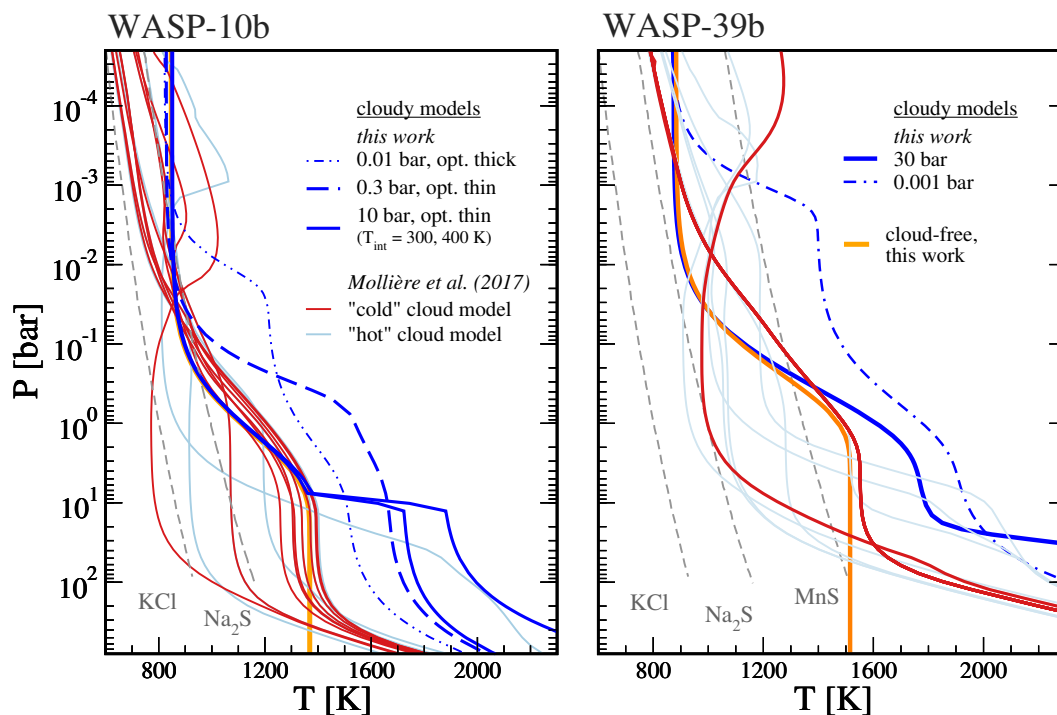
Figure 11. Atmospheric temperature structures for WASP-10b (left) and WASP-39b (right). Our result for the clear atmosphere is shown in orange for $T_{int} = 0$ K as well some of our cloudy solutions in dark blue. The bunch of profiles in red (*cold models*) and light blue (*hot models*) are from Mollière et al. (2017) for different cloud model parameter, see text. The condensation curves assume solar elemental abundance.

6. Conclusions

We performed coupled atmosphere, interior, and evolution calculations for the two giant planets WASP-10b and WASP-39b and investigated the effect of additional absorbers, which we call cloud

decks, of the inferred metallicity. We assumed cloud optical thicknesses of $\tau_c \approx 1$–10 (named optically thin) and $\tau_c \approx 1$–100 (named optically thick), as well as different cloud heights in the atmosphere corresponding to certain condensible species. The clouds decks are purely absorbing and based on the model of Heng et al. (2012) [11]. Our major findings are as follows:

(I)　Through their additional infrared opacity, these cloud decks tend to warm the atmosphere beneath. This leads to a more or less pronounced enhancement in inferred heavy element abundance.

(II)　For the optically thicker cloud decks, the heating is too strong so that condensible species would no longer condense out. This puts an upper limit on the enhancement in metallicity of 100% on both planets.

(III)　For optically thin clouds, the heating of the atmosphere can be sufficiently small so that condensible species can condense out. In this case, we find an increase of the core mass of up to 10% for WASP-10b.

(IV)　For WASP-39b we find a maximum atmospheric metallicity of $Z_{env} = 0.31$ if we assume a deep cloud at 30 bars in the troposphere that in addition would lead to inhibited convection. Even in this favored case, the possible envelope metallicity is still near the lower limit of the observationally inferred value. Further effects that lead to a heating of the planet are clearly required. Since the heating efficiency is empirically not yet constrained, as it is for hot Jupiters [45], $\epsilon > 3\%$ is not excluded for such planets. Such high values would help to bring the observationally inferred Z in agreement with interior-model inferred Z.

Due to the complexity of modeling clouds in a realistic manner, we applied a simple cloud model that is a crude representation of real cloud decks. The predictive power of that model stands and falls with the assumed cloud opacity, cloud height, and cloud thickness, which are poorly known parameters. Another important point is how to couple this cloud model to the atmospheric structure self-consistently. Nevertheless, this work suggests that deep cloud decks below the pressure level accessible to transmission spectra observations may influence the temperature structure in the atmosphere and the inferred metallicity to some extent. A more sophisticated approach is desired.

References

1. Venturini, J.; Alibert, Y.; Benz, W. Planet formation with envelope enrichment: New insights on planetary diversity. *A&A* **2016**, *596*, A90.

2. Wakeford, H.R.; Sing, D.K.; Deming, D.; Lewis, N.K.; Goyal, J.; Wilson, T.J.; Barstow, J.; Kataria, T.; Drummond, B.; Evans, T.M.; et al. The complete transmission spectrum of WASP-39b with a precise water constraint. *Astron. J.* **2018**, *155*, 29. [CrossRef]

3. Thorngren, D.; Fortney, J.J. Connecting giant planet atmosphere and interior modeling: constraints on atmospheric metal enrichment. *Astrophys. J. Lett.* **2019**, *874*, 6. [CrossRef]

4. Maciejewski, G.; Raetz, S.; Nettelmann, N.; Seeliger, M.; Adam, C.; Nowak, G.; Neuhäuser, R. Analysis of new high-precision transit light curves of WASP-10 b: starspot occultations, small planetary radius, and high metallicity. *A&A* **2011**, *535*, A7.

5. Thorngren, D.P.; Fortney, J.J.; Murray-Clay, R.A.; Lopez, E.D. The mass-metallicity relation for giant planets. *Astrophys. J.* **2016**, *831*, 64. [CrossRef]

6. Morley, C.V.; Fortney, J.J.; Kempton, E.M.-R.; Marley, M.S.; Visscher, C.; Zahnle, K. Quantitatively assessing the role of clouds in the transmission spectrum of GJ 1214b. *Astrophys. J.* **2013**, *775*, 33. [CrossRef]

7. Lines, S.; Mayne, N.J.; Boutle, I.A.; Manners, J.; Lee, G.K.H.; Helling, C.; Drummond, B.; Amundsen, D.S.; Goyal, J.; Acreman, D.M.; et al. Simulating the cloudy atmospheres of HD 209458 b and HD 189733 b with the 3D Met Office Unified Model. *A&A* **2018**, *615*, A97.

8. Miller-Ricci, E.; Seager, S.; Sasselov, D. The Atmospheric Signatures of Super-Earths: How to Distinguish Between Hydrogen-Rich and Hydrogen-Poor Atmospheres. *Astrophys. J.* **2009**, *690*, 1056. [CrossRef]

9. Thorngren, D.P.; Gao, P.; Fortney, J.J. The intrinsic temperature and radiative-convective boundary depth in the atmospheres of hot Jupiters. *Astrophys. J. Lett.* **2019**, *884*, L6. [CrossRef]

10. Podolak, M.; Helled, R.; Schubert, G. Effect of non-adiabatic thermal profiles on the inferred composition of Uranus and Neptune. *Mon. Not. R. Astron. Soc.* **2019**, *487*, 2653–2664. [CrossRef]

11. Heng, K.; Hayek, W.; Pont, F.; Sing, D.K. On the effects of clouds and hazes in the atmospheres of hot Jupiters: Semi-analytical temperature-pressure profiles. *Mon. Not. R. Astron. Soc.* **2012**, *420*, 20–36. [CrossRef]

12. Linder, E.F.; Mordasini, C.; Mollière, P.; Marleau, G.D.; Malik, M.; Quanz, S.P.; Meyer, M.R. Evolutionary models of cold and low-mass planets: Cooling curves, magnitudes, and detectability. *A&A* **2019**, *623*, A85.

13. Kurosaki, K.; Ikoma, M. Acceleration of Cooling of Ice Giants by Condensation in Early Atmospheres. *Astron. J.* **2017**, *153*, 260. [CrossRef]

14. Barman, T.S.; Hauschildt, P.H.; Allard, F. Irradiated Planets. *Astrophys. J.* **2001**, *556*, 885–895. [CrossRef]

15. Baraffe, I.; Chabrier, G.; Barman, T.S.; Allard, F.; Hauschildt, P.H. Evolutionary models for cool brown dwarfs and extrasolar giant planets. The case of HD 209458. *A&A* **2003**, *402*, 701–712.

16. Kataria, T.; Sing, D.K.; Lewis, N.K.; Visscher, C.; Showman, A.P.; Fortney, J.J.; Marley, M.S. The atmospheric circulation of a nine-hot-Jupiter sample: Probing circulation and chemistry over a wide phase space. *Astrophys. J.* **2016**, *821*, 9. [CrossRef]

17. Mollière, P.; van Boekel, R.; Bouwman, J.; Henning, T.; Lagage, P.O.; Min, M. Observing transiting planets with JWST. Prime targets and their synthetic spectral observations. *A&A* **2017**, *600*, A10.

18. Johnson, J.A.; Winn, J.N.; Cabrera, N.E.; Carter, J.A. A smaller radius for the transiting exoplanet WASP-10b. *Astrophys. J. Lett.* **2009**, *692*, L100–L104. [CrossRef]

19. Christian, D.J.; Gibson, N.P.; Simpson, E.K.; Street, R.A.; Skillen, I.; Pollacco, D.; Collier Cameron, A.; Joshi, Y.C.; Keenan, F.P.; Stempels, H.C.; et al. WASP-10b: A 3MJ, gas-giant planet transiting a late-type K star. *Mon. Not. R. Astron. Soc.* **2009**, *392*, 1585. [CrossRef]

20. Maciejewski, G.; Dimitrov, D.; Neuhäuser, R.; Tetzlaff, N.; Niedzielski, A.; St. Raetz; Chen, W.P.; Walter, F.; Marka, C.; Baar, S.; et al. Transit timing variation and activity in the WASP-10 planetary system. *Mon. Not. R. Astron. Soc.* **2010**, *411*, 1204–1212. [CrossRef]

21. Faedi, F.; Barros, S.C.C.; Anderson, D.R.; Brown, D.J.A.; Collier Cameron, A.; Pollacco, D.; Boisse, I.; Hébrard, G.; Lendl, M.; Lister, T.A.; et al. WASP-39b: A highly inflated Saturn-mass planet orbiting a late G-type star. *A&A* **2011**, *531*, A40.

22. Mordasini, C.; van Boekel, R.; Mollière, P.; Henning, T.; Benneke, B. The imprint of exoplanet formation history on observable present-day spectra of hot Jupiters. *Astrophys. J.* **2016**, *832*, 41. [CrossRef]

23. Lodders, K. Solar system abundances and condensation temperatures of the elements. *Astrophys. J.* **2003**, *591*, 1220. [CrossRef]

24. Saumon, D.; Chabrier, G. An equation of state for low-mass stars and giant planets. *Astrophys. J. Suppl.* **1995**, *99*, 713–741. [CrossRef]

25. Hubbard, W.B.; Marley, M.S. Optimized Jupiter, Saturn, and Uranus interior models. *Icarus* **1989**, *78*, 102. [CrossRef]

26. Nettelmann, N.; Fortney, J.J.; Kramm, U.; Redmer, R. Thermal evolution and structure models of the transiting super-Earth GJ 1214b. *Astrophys. J.* **2011**, *733*, 2. [CrossRef]

27. Fortney, J.J.; Nettelmann, N. The interior structure, composition, and evolution of giant planets. *Space Sci. Rev.* **2010**, *152*, 423–447. [CrossRef]

28. Guillot, T. On the radiative equilibrium of irradiated planetary atmospheres. *A&A* **2010**, *520*, A27.

29. Marley, M.S.; Gelino, C.; Stephens, D.; Lunine, J.I.; Freedman, R. Reflected spectra and albedos of extrasolar giant planets. I. Clear and cloudy atmospheres. *Astrophys. J.* **1999**, *513*, 879–893. [CrossRef]

30. Gelino, G.; Marley, M.; Stephens, D.; Lunine, J.; Freedman, R. Model Bond Albedos of Extrasolar Giant Planets. *Phys. Chem. Earth* **1999**, *24*, 573–578. [CrossRef]

31. Sudarsky, D.; Burrows, A.; Pinto, P. Albedo and reflection spectra of extrasolar giant planets. *Am. Astron. Soc.* **2000**, *538*, 885–903. [CrossRef]

32. Madhusudhan, N.; Knutson, H.; Fortney, J.J.; Barman, T. Exoplanetary atmospheres. In *Protostars and Planets VI*; University of Arizona Press: Tucson, AZ, USA, 2014.

33. Li, L.; Jiang, X.; West, R.A.; Gierasch, P.J.; Perez-Hoyos, S.; Sanchez-Lavega, A.; Fletcher, L.N.; Fortney, J.J.; Knowles, B.; Porco, C.C.; et al. Less absorbed solar energy and more internal heat for Jupiter. *Nat. Commun.* **2018**, *9*, 3709. [CrossRef] [PubMed]

34. Heng, K.; Mendonça, J.M.; Lee, J.M. Analytical models of exoplanetary atmospheres. II. Radiative transfer via the two-stream approximation. *Astrophys. J. Suppl.* **2014**, *215*, 4. [CrossRef]

35. Fortney, J.J.; Marley, M.S.; Barnes, J.W. Planetary radii across five orders of magnitude in mass and stellar insolation: Application to transits. *Astrophys. J.* **2007**, *659*, 1661–1672. [CrossRef]

36. Fortney, J.J.; Saumon, D.; Marley, M.; Lodders, K.; Freedman, R. Atmosphere, Interior, and Evolution of the Metal-rich Transiting Planet HD 149036b. *Astrophys. J.* **2006**, *642*, 495. [CrossRef]

37. Mollière, P.; Van Boekel, R.; Dullemond, C.; Henning, T.; Mordasini, C. Model atmospheres of irradiated exoplanets: The influence of stellar parameters, metallicity, and the C/O ratio. *Astrophys. J.* **2015**, *813*, 47. [CrossRef]

38. Wakeford, H.R.; Visscher, C.; Lewis, N.K.; Kataria, T.; Marley, M.S.; Fortney, J.J.; Mandell, A.M. High-temperature condensate clouds in super-hot Jupiter atmospheres. *Mon. Not. R. Astron. Soc.* **2017**, *464*, 4247. [CrossRef]

39. Valencia, D.; Guillot, T.; Parmentier, V.; Freedman, R.S. Bulk composition of GJ 1214b and other sub-neptune exoplanets. *Astrophys. J.* **2013**, *775*, 10. [CrossRef]

40. Freedman, R.; Marley, M.; Lodders, K. Line and mean opacities for ultracool dwarfs and extrasolar planets. *Astrophys. J. Suppl.* **2008**, *174*, 504–513. [CrossRef]

41. Marley, M.S. The Role of Condensates in L- and T-dwarf Atmospheres. In *From Giant Planets to Cool Stars*; ASP Conference Series; ASP: San Francisco, CA, USA, 2000.

42. Lodders, K.; Fegley, B. Chemistry of low mass substellar objects. In *Astrophysics Update 2*; Springer: Heidelberg, Germany, 2006.

43. Morley, C.V.; Fortney, J.J.; Marley, M.S.; Zahnle, K.; Line, M.; Kempton, E.; Lewis, N.; Cahoy, K. Thermal emission and reflected light spectra of super earths with flat transmission spectra. *Astrophys. J.* **2015**, *815*, 110. [CrossRef]

44. Alexander, R.; Armitage, P. Giant planet migration, disk evolution, and the origin of transitional disks. *Astrophys. J.* **2009**, *704*, 989. [CrossRef]

45. Thorngren, D.P.; Fortney, J.J. Bayesian Analysis of Hot-Jupiter Radius Anomalies: Evidence for Ohmic Dissipation? *Astron. J.* **2018**, *155*, 214. [CrossRef]

46. Leconte, J.; Selsis, F.; Hersant, F.; Guillot, T. Condensation-inhibited convection in hydrogen-rich atmospheres. *A&A* **2017**, *598*, A98.

47. Sing, D.K.; Fortney, J.J.; Nikolov, N.; Wakeford, H.R.; Kataria, T.; Evans, T.M.; Aigrain, S.; Ballester, G.E.; Burrows, A.S.; Deming, D.; et al. A continuum from clear to cloudy hot-Jupiter exoplanets without primordial water depletion. *Nature* **2016**, *529*, 59–62. [CrossRef] [PubMed]

48. Nikolov, N.; Sing, D.K.; Gibson, N.P.; Fortney, J.J.; Evans, T.M.; Barstow, J.K.; Kataria, T.; Wilson, P.A. VLT FORS2 comparative transmission spectroscopy: Detection of Na in the atmosphere of WASP-39b from the ground. *Astrophys. J.* **2016**, *832*, 191. [CrossRef]

49. Becker, A.; Lorenzen, W.; Fortney, J.J.; Nettelmann, N.; Redmer, R.; Schöttler, M. Ab initio equation of state for hydrogen (H-REOS.3) and helium (He-REOS.3) and their implications for the interior of brown dwarfs. *Astrophys. J. Suppl.* **2014**, *215*, A21. [CrossRef]

50. Chabrier, G.; Baraffe, I. Heat transport in giant (exo)planets: A new perspective. *Astrophys. J. Lett.* **2007**, *661*, L81–L84. [CrossRef]

51. Leconte, J.; Chabrier, G. Layered convection as the origin of Saturn's luminosity anomaly. *Nat. Geosci.* **2013**, *6*, 347–350. [CrossRef]

52. Malik, M.; Kitzmann, D.; Mendonça, J.; Grimm, S.; Marleau, G.D.; Linder, E.; Tsai, S.M.; Heng, K. Self-luminous and Irradiated Exoplanetary Atmospheres Explored with HELIOS. *Astron. J.* **2019**, *157*, 170. [CrossRef]

53. Allard, F.; Hauschildt, P.; Alexander, D.; Tamanai, A.; Schweitzer, A. The Limiting Effects of Dust in Brown Dwarf Model Atmospheres. *Astrophys. J.* **2001**, *556*, 357. [CrossRef]

54. Hauschildt, P.; Baron, E. Numerical Solution of the Expanding Stellar Atmosphere Problem. *J. Comput. Appl. Math.* **1999**, *109*, 41. [CrossRef]

55. Ackerman, A.; Marley, M. Precipitating condensation clouds in substellar atmospheres. *Astrophys. J.* **2001**, *556*, 872. [CrossRef]